

A COHERENT TIMING SOLUTION FOR THE NEARBY, THERMALLY EMITTING ISOLATED NEUTRON STAR RX J0420.0–5022

D. L. KAPLAN¹ AND M. H. VAN KERKWIJK²
ApJL, in press

ABSTRACT

We present a phase-coherent timing solution for RX J0420.0–5022, the coolest ($kT \simeq 45$ eV) and fastest-spinning ($P = 3.45$ s) of the seven so-called isolated neutron stars (INSs). Using 14 observations with the *XMM-Newton* spacecraft in 2010–2011, we were able to measure a spin-down rate $\dot{\nu} = (-2.3 \pm 0.2) \times 10^{-15} \text{ Hz s}^{-1}$ ($\dot{P} = (2.8 \pm 0.3) \times 10^{-14} \text{ s s}^{-1}$), from which we infer a dipolar magnetic field of 1.0×10^{13} G. With reasonable confidence we were able to extend the timing solution back to archival *XMM-Newton* from 2002 and 2003, giving the same solution but with considerably more precision. This gives RX J0420.0–5022 the lowest dipole magnetic field of the INSs. Our spectroscopy does not confirm the broad absorption feature at 0.3 keV hinted at in earlier observations, although difficulties in background subtraction near that energy make conclusions difficult. With this, all 6 of the INSs that have confirmed periodicities now have constrained spin-downs from coherent solutions. The evidence that the INSs are qualitatively different from rotation-powered pulsars now appears robust, with the likely conclusion that their characteristic ages are systematically older than their true ages, because their fields have decayed. The field decay probably also causes them to be systematically hotter than pulsars of the same (true) age.

Subject headings: stars: individual (RX J0420.0–5022) — stars: neutron — X-rays: stars

1. INTRODUCTION

The so-called isolated neutron stars (INSs; see Haberl 2007 and Kaplan 2008 for reviews) are a group of seven nearby ($\lesssim 1$ kpc) neutron stars with low ($\sim 10^{32} \text{ erg s}^{-1}$) X-ray luminosities and long (3–10 s) spin periods (Kaplan & van Kerkwijk 2009b). They are unique in that the X-ray emission likely comes from a large fraction of the neutron stars' surfaces, and is not influenced by accretion (as in the case of X-ray binaries) or non-thermal magnetospheric emission (as in the case of rotation-powered pulsars); the INSs are also radio-quiet (e.g., Kondratiev et al. 2009). The INSs then have the potential to help understand neutron star radii and cooling via measurements of their emission areas and luminosities, but this is made difficult by our inability to realistically model the X-ray, ultra-violet, and optical emission from these objects (e.g., Ho et al. 2007; Kaplan et al. 2011).

Recently it was proposed (Kaplan & van Kerkwijk 2009b; Pons, Miralles, & Geppert 2009; Popov et al. 2010) that the current temperatures and magnetic fields of the INSs reflect non-thermal, coupled evolution, where the magnetic field has decayed in strength, heating the neutron-star surface. Testing this hypothesis is an important step to using the INSs to constrain the overall cooling history of neutron stars, and through it probe their inner structure and composition (Yakovlev & Pethick 2004). To constrain evolutionary models, measurements of the current magnetic fields and temperatures of the INSs are required. Similarly, to understand

the broad absorption features seen at energies of 0.2–0.75 keV in the spectra of almost all INSs (Haberl 2007; van Kerkwijk & Kaplan 2007), also requires knowledge of the magnetic fields, as at these field strengths the assumed transition energies are field-dependent. Therefore, we have undertaken systematic measurements of the dipole magnetic fields for the INSs through phase-coherent X-ray timing using the *Chandra* and *XMM-Newton* spacecraft (Kaplan & van Kerkwijk 2005a,b; van Kerkwijk & Kaplan 2008; Kaplan & van Kerkwijk 2009a,b, hereafter KvK05a; KvK05b; vKK08; KvK09; KvK09b).

Here we measure the spin-down of the INS RX J0420.0–5022 (hereafter RX J0420), the last INS with a confirmed period measurement but without a timing solution. RX J0420 was identified as a possible neutron star by Haberl, Pietsch, & Motch (1999), although it had originally been associated with a nearby galaxy. Followup *ROSAT* observations showed a very soft thermal spectrum and yielded an improved position, both of which led to its classification as a neutron star. While initially a 22.7-s period was suggested, observations with *XMM* found a period of 3.45 s instead, the shortest among all INSs (Haberl et al. 2004, hereafter H+04); the same observations also showed that RX J0420 was the coolest INS, with $kT \simeq 45$ eV.

2. OBSERVATIONS & ANALYSIS

We observed RX J0420 fourteen times with *XMM* (Jansen et al. 2001) in 2010 and 2011, and focus here on the data taken with the European Photon Imaging Camera (EPIC) with pn and MOS detectors, all used in small window mode with thin filters (Table 1). We reprocessed our observations with SAS version 11.0.0 and calibration files current as of 2011 May 25. We also reprocessed the pn data from H+04, which are taken with

¹ Physics Dept., U. of Wisconsin - Milwaukee, Milwaukee WI 53211, USA; kaplan@uwm.edu

² Department of Astronomy and Astrophysics, University of Toronto, 60 St. George Street, Toronto, ON M5S 3H8, Canada; mhvk@astro.utoronto.ca

TABLE 1
LOG OF OBSERVATIONS AND TIMES OF ARRIVAL

Rev.	Date	Exp. ^a (ks)	Counts ^a	f_{bg} ^a (%)	TOA ^b (MJD TDB)
560	2002 Dec 30	20,047	4,201	10.0	52638.2855519(12)
561	2002 Dec 31	20,048	4,593	11.7	52640.0466236(12)
570	2003 Jan 19	20,547	4,647	11.6	52658.8319656(8)
664	2003 Jul 25	20,036	4,384	11.8	52846.0226435(10)
1887	2010 Mar 30	7,472	2,062	41.2	55285.5413317(17)
1890	2010 Apr 04	9,072	2,679	45.8	55290.8432112(23)
1892	2010 Apr 09	7,772	2,049	35.4	55295.4037368(11)
1913	2010 May 21	5,471	1,462	32.1	55337.2761247(20)
1948	2010 Jul 29	6,472	1,626	37.2	55406.6382597(30)
1975	2010 Sep 21	9,872	2,372	38.2	55460.4233059(20)
1981	2010 Oct 02	11,672	2,980	34.8	55472.0349984(22)
1981	2010 Oct 03	12,972	3,064	38.6	55472.8839787(11)
1981	2010 Oct 04	16,871	4,465	40.2	55473.3194015(13)
1983	2010 Oct 06	10,471	2,586	36.9	55476.0218532(19)
2008	2010 Nov 26	5,471	1,339	35.2	55526.4316848(19)
2032	2011 Jan 13	15,471	4,223	44.5	55575.0260821(17)
2071	2011 Mar 31	7,018	1,577	38.2	55651.9068660(24)
2076	2011 Apr 11	5,471	1,248	32.2	55662.3338203(19)

NOTE. — All observations used the small window mode and thin filter for both EPIC-pn and EPIC-MOS1/2, except for Revs. 560, 561, 570, 664, in which the full window mode was used (which meant that only the EPIC-pn data were suitable for timing).

^a The exposure time, number of counts, and estimated fraction of events due to background f_{bg} given here are for EPIC-pn only.

^b The TOA is defined as the time of maximum light of the fundamental closest to the middle of each observation computed from the combined EPIC-pn and EPIC-MOS1/2 datasets, and is given with 1- σ uncertainties.

the same filter, but with the full window mode instead (we did not use their full-frame MOS data, since these do not resolve the pulsations). We used `epchain` and `emchain` and selected source events from a circular region of 37.5 radius. For the pn, we selected energies between 130 and 800 eV, where we set our lower energy cutoff slightly below the default of 150 eV to increase the net number of counts from our very soft target (by about 25%; for even lower thresholds, the instrumental background increases too rapidly), and the upper cutoff at the energy at which the source becomes undetectable (thus minimizing the effects of flares, which dominate the background at higher energies). Following standard practice, we included only one and two-pixel (single and double patterns 0–4) events with no warning flags for pn, and single, double, and triple events (patterns 0–12) with the default flag mask for MOS1/2. We barycentered the event times using the *Chandra X-ray Observatory* position from H+04: $\alpha = 04^{\text{h}}20^{\text{m}}01^{\text{s}}.95$ and $\delta = -50^{\circ}22'48''.1$ (J2000). We extracted background lightcurves for pn from similarly sized regions offset from the source, but at the same RAWY coordinate, as recommended by the SAS User Guide.³ For MOS1/2, the small-window mode does not permit such large background areas, but we used several smaller areas to compensate.

2.1. Timing Analysis

Our timing analysis largely follows the procedure described in KvK05a. As a starting place, we first determined the frequency that maximized the power in a Z_1^2 periodogram for the EPIC-pn data from the

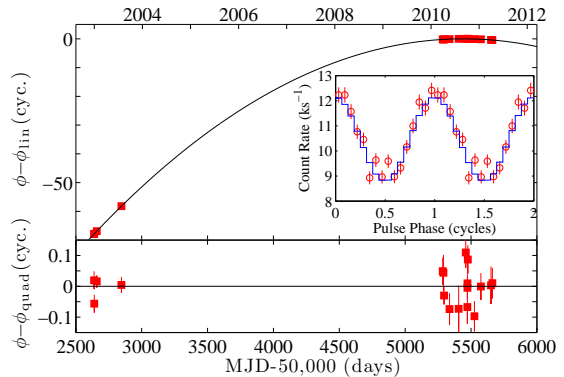


FIG. 1.— Phase residuals for RX J0420. In the top panel, we show the residuals relative to a linear model ($\dot{\nu} = 0$). The line shows the best-fit quadratic solution. Residuals relative to the quadratic solution are shown in the bottom panel. Inset: pulse profile for RX J0420, based on a combination of all of the 2010–2011 data folded according to the ephemeris in Tables 2 and corrected for the background. The blue curve is the best-fit sinusoidal profile.

longest observation in Rev. 1981. We then expanded the periodogram to include data from all observations in Revs. 1981 and 1983, finding a best-fit frequency of $\nu = 0.2896033 \pm 0.0000003$ Hz, consistent with that found by H+04 for the earlier data. In contrast to some of the other INSSs, there is no evidence for higher harmonics in the periodogram: the Z_1^2 power is 33.8, while $Z_2^2 = 34.7$ and $Z_3^2 = 35.2$, both of which are consistent with the additional power of 1 expected for noise. We also checked to see if the true period was in fact 6.9 s (closer to that of the other INSSs), but the pulse shape, hardness ratio, and median energy were all consistent with no variation between the first and second halves of the pulse (with 16 bins the lightcurve variation between the first and second halves has $\chi^2 = 10.6/8$, while the hardness ratio variation has $\chi^2 = 4.1/8$).

Using the above frequency, we determined the times-of-arrival (TOAs; see Table 1) for the combined EPIC data from each observation by fitting the binned lightcurves (following KvK05b) to a single sinusoid, appropriate given the results of the periodograms (Fig. 1); the best-fit sinusoid to the composite, background corrected pn data had a semi-amplitude of $15 \pm 2\%$, where the uncertainty includes an estimate for the variation in the background correction over different background regions. This is a little higher than the semi-amplitude of about 10% from H+04, but differences in background-subtraction and energy selection could account for the difference (our best-fit to the 2002–2003 data has a semi-amplitude of $13.2 \pm 1.1\%$). The χ^2 for the fit to the composite profile was good, 14.4 for 13 dof.

Using our TOAs, we were able to identify a reasonably unambiguous coherent timing solution. This was possible as we restricted solutions to have $|\dot{\nu}| < 9 \times 10^{-13}$ Hz s⁻¹ or $B_{\text{dip}} < 2 \times 10^{14}$ G (based on the incoherent limits set by Haberl 2007). Among those, the solution presented in Table 2 was the best, yielding $\chi^2 = 19.9$ for 11 degrees of freedom, with alternatives at $\chi^2 = 25.1$ ($B_{\text{dip}} = 1.8 \times 10^{14}$ G), $\chi^2 = 37.3$ ($B_{\text{dip}} = 7 \times 10^{13}$ G), and $\chi^2 = 38.5$ ($\dot{\nu} > 0$). Of these, all but the first can be excluded on statistical grounds. The first comes from an uncertainty of 0.1 cycle in the cycle count between the

³ See http://xmm.esac.esa.int/external/xmm_user_support/documentation/sas_users/USG/node64.html

TABLE 2
MEASURED AND DERIVED TIMING PARAMETERS FOR
RX J0420.0–5022

Quantity	Value	
	2010–2011	2002–2011
Dates (MJD) ..	55,286–55,662	52,638–55,662
t_0 (MJD).....	55,430.6001387(6)	55430.6001387(6)
ν (Hz)	0.2896029061(12)	0.2896029058(10)
$\dot{\nu}$ (10^{-15} Hz s $^{-1}$)	-2.3(2)	-2.314(8)
TOA rms (s) ...	0.3	0.2
χ^2 /DOF	19.9/11	24.8/15
\dot{P} (s).....	3.453004024(14)	3.453004027(12)
\dot{P} (10^{-14} s s $^{-1}$)	2.8(3)	2.759(10)
τ_{char} (Myr).....	2.0	2.0
B_{dip} (10^{13} G) ..	1.0	1.0
\dot{E} (10^{31} erg s $^{-1}$)	2.7	2.7

NOTE. — Quantities in parentheses are the formal 1- σ uncertainties on the last digit. $\tau_{\text{char}} = P/2\dot{P}$ is the characteristic age, assuming an initial spin period $P_0 \ll P$ and a constant magnetic field; $B_{\text{dip}} = 3.2 \times 10^{19} \sqrt{P\dot{P}}$ G is the magnetic field inferred assuming spin-down by dipole radiation; $\dot{E} = 3.9 \times 10^{46} \nu \dot{\nu}$ erg s $^{-1}$ is the spin-down luminosity.

densely sampled Rev. 1981–1983 group and the next closest observation, Rev. 1975, and is close to the limit from Haberl (2007); we will return to this alias shortly. We were able to identify the same solution using a single coherent $Z_1^2(\nu, \dot{\nu})$ periodogram (as in vKK08). Spin-down is well-detected, at $\sim 10\sigma$. The reduced χ^2 is somewhat high, but even adjusting our uncertainties to allow for an reduced χ^2 of 1 will still give an 8σ detection of spin-down. The implied magnetic field is well within the range of other detections for the INSSs (KvK09b).

We can confirm and improve our solution by extrapolating it back to the older data from 2002–2003. The time difference is roughly 2600 days and our $\dot{\nu}$ uncertainty gives a formal cycle-count uncertainty of ± 5 cycles, but by trying multiple solutions, we find that only a single cycle count difference leads to a solution that fits all four earlier TOAs. Trying this generally, iteratively exploring all cycle-count ambiguities between all data sets, we find a single best-fit solution that agrees with the best-fit solution using only the new data (Table 2 and Figure 1). With $\chi^2 = 24.8$ for 15 degrees-of-freedom, it still has a slightly high reduced χ^2 . However, the alternate solutions either have nearly the same implied spin-down rate but differ slightly in the cycle counts between the 2002–2003 and 2010–2011 observations (and the lowest of those has $\chi^2 = 33.0$), or are dramatically different but have significantly worse χ^2 ($\chi^2 = 45.9$ and $\dot{\nu} > 0$). The alternate, $B_{\text{dip}} = 1.8 \times 10^{14}$ G solution from above does not extrapolate well to the older data, allowing us to exclude it. Overall, the older data thus allow us to confidently select the correct solution to the new data, and select a reasonably secure overall solution ($\Delta\chi^2 = 8.1$).

2.2. Spectroscopic Analysis

We examined all EPIC-pn spectra of RX J0420. (A full spectral analysis, including the EPIC-MOS and RGS data and a phase-resolved analysis, is in progress.) We used the same source and background extraction regions as for the timing analysis, created appropriate response

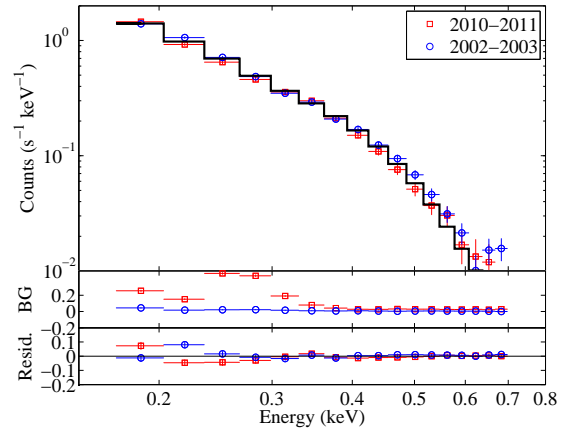


FIG. 2.— Blackbody fits to the merged EPIC-pn data of RX J0420, from 2002–2003 (blue circles) and 2010–2011 (red squares). The model is the thick black line. The middle panel shows the backgrounds used, and highlights the background structure seen at low energies in the 2010–2011 data. The bottom panel shows the residuals.

files, and binned the spectral files such that the number of source plus background counts was at least 25 and the bin width was at least 30 eV (so that there are roughly 2 bins per EPIC-pn resolution element).

We first compared the raw EPIC-pn spectra of all of the observations against each other. This did not include any response files or calibration corrections, but even so the binned pn spectra were generally consistent with each other, implying no spectral change (Fig. 2). There are small deviations at low energies (0.2–0.4 keV) and we will return to these below, but the 2010–2011 data did not show any appreciable variability.

We fit the pn data using *sherpa* (Refsdal et al. 2009). To aid in fitting we merged the event and response files into two groups: one for 2002–2003 (full-frame data, also fit by H+04) and one for 2010–2011 (small-window data). While not perfect, we found that an absorbed blackbody provided a reasonable fit, with $N_{\text{H}} < 1 \times 10^{18}$ cm $^{-2}$, $kT_{\infty} = 47.6 \pm 0.3$ eV, and $R_{\infty} = 12.8 \pm 0.3$ km kpc $^{-1}$ (formal 1- σ uncertainties; $\chi^2 = 73.0$ for 31 dof), reasonably consistent with H+04. Unlike H+04, we do not find evidence for a spectral feature, perhaps because of changes in the response files and calibration since earlier fits. However, there are indications that our fit is not completely reliable. First, the best-fit value of the absorption is 0 (although it is covariant with the blackbody temperature). Second, there are some residuals near 0.33 keV, where H+04 found evidence for a spectral line. However, we could not find a consistent fit to both sets of data. Third, stronger differences are seen at energies of 0.2–0.3 keV (see Figure 2). Some of these are too narrow to come from astrophysical sources, and instead likely reflect problems in background subtraction (the low-energy background for the small-window data in particular can be significant and has substantial energy structure⁴). Hence, it is difficult to interpret any residual structure there with respect to a blackbody.

3. DISCUSSION & CONCLUSIONS

We have determined a reliable, statistically significant coherent spin-down solution for RX J0420. With this,

⁴ See [http://www.star.le.ac.uk/\\$\sim\\$amr30/BG/BGTable.html](http://www.star.le.ac.uk/\simamr30/BG/BGTable.html).

only RX J1605.3+3249, which as yet has only a tentative detection of a periodicity, lacks a coherent solution (although in the cases of RX J2143.0+0654 and RX J0806.4–4123 spin-down was not well measured, and further observations are in progress). While the overall results of our timing program have been discussed at length in previous papers (overall energetics in vKK08; spectral implications in KvK09; evolutionary models in KvK09b), here we touch on some of the aspects that make RX J0420 unique and compare it to the other objects in its class.

First, while the timing properties (dipole magnetic field, \dot{E} , characteristic age) of RX J0420 place it well within the INSs, RX J0420 has the shortest period by more than a factor of 2. In the context of the magnetothermal evolution model, this could be a consequence of a lower initial magnetic field, and thus less dramatic early spin-down. RX J0420 also has the lowest current field, although it is not clear whether there is a good correlation between current magnetic field and period: RX J0806.4–4123 and RX J2143.0+0654 both have long periods but relatively weak magnetic fields. The magnetic field of RX J0420 is low enough that it would not be remarkable in a radio pulsar.

Second, the temperature of RX J0420 is the lowest of the INSs. Again, this might make sense if it is roughly the same age as the rest of the INSs but started with the lowest magnetic field. It would then have been heated the least, and would come closest to the “pristine” cooling of a non-magnetic neutron star. In this context, it is interesting that RX J1856.5–3754 is cooler and less magnetized than RX J0720.4–3125 (1.5 vs 2.5×10^{13} G), while appearing the younger one by kinematic age (Kaplan, van Kerkwijk, & Anderson 2007; Tetzlaff et al. 2010, 2011). It would be interesting to measure the kinematic age of RX J0420 to compare it with the rest of the population.

To view the evidence for field decay in a different way, we show in Figure 3 the blackbody temperature versus characteristic age for pulsars and the INSs (see also Zhu et al. 2011). It is quite clear that the INSs are systematically a factor of 5–10 older in characteristic age for the same temperature. If instead one uses the kinematic age, however, one sees that the difference is much smaller (for the two sources for which kinematic ages are available). In the context of a picture in which the fields of INSs decayed, the main difference with pulsars induced by the initially much stronger field is thus that it leads to rapid initial spin down and long present periods (and thus long characteristic ages); the current temperatures are not as strongly affected. Indeed, in the models of Pons et al. (2009), the heat generated by field decay is lost fairly rapidly.

Third, given both the low temperature and low magnetic field, RX J0420 largely follows the empirical temperature-magnetic field correlation from KvK09. As discussed there, the origin of this relation (evolutionary vs. surface physics) or even its overall integrity in the face of new data are not clear. It does seem to form an upper limit to the possible magnetic field of an INS, and even the rotating radio transient (RRAT) J1819–1458 (possibly somewhat younger than the INSs, and with higher \dot{E} as well) seems to roughly agree (based

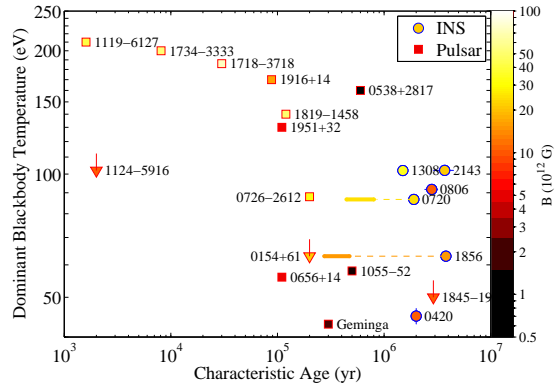


FIG. 3.— Blackbody temperature (measured at infinity) versus characteristic age for the INSs (circles) and rotation-powered pulsars (squares and upper limits); for all objects the color indicates the dipole magnetic field according to the scale at the right. The pulsars included here are both those that are visible in the *ROSAT* All-Sky Survey and those with dipole fields $\geq 10^{13}$ G that have X-ray measurements. See Zhu et al. (2011) for a similar plot, although there they emphasize the variation among radio pulsars as a function of magnetic field, while here we emphasize primarily the distinction between pulsars and INSs. The data are taken from Kaplan & van Kerkwijk (2009b), with the addition of PSR B1916+14 (Zhu et al. 2009), PSR J1734–3333 (Olausen et al. 2010), an updated temperature for PSR J1718–3718 (Zhu et al. 2011), an upper limit for PSR B1845–19 (Zhu et al. 2011, in prep), PSR J0726–2612 (Kaplan et al., in prep.), an updated timing solution for RX J0806.4–4123 (van Kerkwijk et al., in prep.), and data from this paper. We only show data for sources where the blackbody can plausibly represent the majority of the surface (i.e., $R_{\text{BB}} > 3$ km, allowing for distance uncertainties). This is not meant to be a cooling curve, but instead to demonstrate the inconsistency in characteristic ages for the INS relative to the pulsars at the same kT . The horizontal lines extending to the left of RX J1856.5–3754 and RX J0720.4–3125 show the ranges of plausible kinematic ages (Kaplan et al. 2007; Tetzlaff et al. 2011) for those objects, with the thick parts the mostly likely ranges.

on McLaughlin et al. 2007).

Fourth, we did not confirm the tentative absorption feature found by H+04, although problems with the background subtraction meant we cannot refute it with confidence either. If it is true that RX J0420 has no broad X-ray absorption feature, it would join RX J1856.5–3754 (although as this object is often used for calibration *assuming* it emits like a blackbody, it is difficult to set confident limits). These are the two INSs with the lowest temperatures and the lowest magnetic fields, suggesting some relation between the presence of absorption features (or their energy) and either temperature or field strength (although a direct correlation of energy with field strength seems excluded; KvK09). RX J0420 is also similar to RX J1856.5–3754 in its optical excess: both are reasonably well fit by Rayleigh-Jeans like powerlaws, unlike the other INSs whose spectra are softer (Kaplan et al. 2011). It is possible that the optical/UV spectral index is related to the magnetic field, either directly through the magnetosphere (Tong et al. 2011) or indirectly through shifting spectral lines (Kaplan et al. 2011); in that case the similarity of RX J0420 and RX J1856.5–3754 would be natural.

Overall, our measurement firmly places RX J0420 as one of the INSs despite its short period, and moves us significantly closer to having a complete sampled of measured spin-downs for that population. There are still a number of open questions to be answered via X-ray and multi-wavelength observations. Primary among these

is understanding the surface emission through consistent modeling of the spectra and lightcurves, and ideally with phase-resolved spectroscopy. Observations at optical/UV wavelengths of the pulsed emission could make significant improvements in our understanding, by tying the emitting areas at different wavelengths together and establishing the degree of surface inhomogeneity. Finally, further kinematic ages would help greatly in constraining the coupled evolution of magnetic field and temperature.

Based on observations obtained with XMM-Newton, an ESA science mission with instruments and contributions directly funded by ESA Member States and NASA. DLK was partially supported by NASA through grant NNX08AX39G. Apart from the XMMSAS data reduction pipelines provided by *XMM-Newton*, this research has made use of software provided by the Chandra X-ray Center (CXC) in the application packages CIAO and Sherpa.

REFERENCES

- Haberl, F. 2007, *Ap&SS*, 308, 181
Haberl, F., et al. 2004, *A&A*, 424, 635
Haberl, F., Pietsch, W., & Motch, C. 1999, *A&A*, 351, L53
Ho, W. C. G., Kaplan, D. L., Chang, P., van Adelsberg, M., & Potekhin, A. Y. 2007, *MNRAS*, 375, 821
Jansen, F., et al. 2001, *A&A*, 365, L1
Kaplan, D. L. 2008, *AIPC*, 983, 331, arXiv:0801.1143
Kaplan, D. L., Kamble, A., van Kerkwijk, M. H., & Ho, W. C. G. 2011, *ApJ*, 736, 117
Kaplan, D. L. & van Kerkwijk, M. H. 2005a, *ApJ*, 628, L45 (KvK05a)
—, 2005b, *ApJ*, 635, L65 (KvK05b)
—, 2009a, *ApJ*, 692, L62 (KvK09)
—, 2009b, *ApJ*, 705, 798 (KvK09b)
Kaplan, D. L., van Kerkwijk, M. H., & Anderson, J. 2007, *ApJ*, 660, 1428
Kondratiev, V. I., McLaughlin, M. A., Lorimer, D. R., Burgay, M., Possenti, A., Turolla, R., Popov, S. B., & Zane, S. 2009, *ApJ*, 702, 692
Lo Curto, G., Mignani, R. P., Perna, R., & Israel, G. L. 2007, *A&A*, 473, 539
McLaughlin, M. A., et al. 2007, *ApJ*, 670, 1307
Olausen, S. A., Kaspi, V. M., Lyne, A. G., & Kramer, M. 2010, *ApJ*, 725, 985
Pons, J. A., Miralles, J. A., & Geppert, U. 2009, *A&A*, 496, 207
Popov, S. B., Pons, J. A., Miralles, J. A., Boldin, P. A., & Posselt, B. 2010, *MNRAS*, 401, 2675
Posselt, B., Neuhauser, R., & Haberl, F. 2009, *A&A*, 496, 533
Refsdal, B., et al. 2009, in *Proceedings of the 8th Python in Science conference (SciPy 2009)*, ed. G. Varoquaux, S. van der Walt, & J. Millman, 51–57
Tetzlaff, N., Eisenbeiss, T., Neuhaeuser, R., & Hohle, M. M. 2011, *MNRAS*, in press, arXiv:1107.1673
Tetzlaff, N., Neuhauser, R., Hohle, M. M., & Maciejewski, G. 2010, *MNRAS*, 402, 2369
Tong, H., Xu, R. X., & Song, L. M. 2011, *Research in Astronomy and Astrophysics*, submitted, arXiv:1107.0830
van Kerkwijk, M. H. & Kaplan, D. L. 2007, *Ap&SS*, 308, 191
—, 2008, *ApJ*, 673, L163 (vKK08)
Yakovlev, D. G. & Pethick, C. J. 2004, *ARA&A*, 42, 169
Zhu, W., Kaspi, V. M., Gonzalez, M. E., & Lyne, A. G. 2009, *ApJ*, 704, 1321
Zhu, W. W., Kaspi, V. M., McLaughlin, M. A., Pavlov, G. G., Ng, C.-Y., Manchester, R. N., Gaensler, B. M., & Woods, P. M. 2011, *ApJ*, 734, 44